7 Morphological Features of Basal Cell Carcinoma on Ex Vivo Confocal Imaging and Histopathologic Correlation

Mercedes Sendín-Martín, Ucalene Harris, Matthew Moronta, Melissa Pulitzer, Erica Lee, Anthony Rossi, Chih-Shan Jason Chen, Kishwer Nehal, and Manu Jain

Abstract

Basal cell carcinoma is the most common skin cancer worldwide. Mohs micrographic surgery (MMS) is a specialized surgical procedure to treat and achieve complete clearance of BCCs. However, frozen sectioning performed during MMS is a time-consuming and a labor-intensive process. Ex vivo confocal microscopy (EVCM) is an attractive alternative to frozen sectioning during MMS as it can rapidly image fresh (unprocessed and un-sectioned) tissue, enabling tumor margin assessment in real-time. EVCM has shown high sensitivity and specificity for detecting BCCs. In this chapter, we have described the morphological features of common subtypes of BCC as visualized in various imaging modes on the EVCM (fluorescence confocal microscopy and digital H&E mode) and compared them with their corresponding.

Basal cell carcinoma (BCC) is the most common skin cancer worldwide [1]. Annually, two million new BCC cases are estimated in the USA [2], and the incidence rates are expected to rise due to aging population [3]. Exposure to UV radiation from sunlight is the primary etiologic agent for BCC, particularly among individuals with lighter skin prototypes (I to III) (Table 7.1).

Although BCCs are indolent tumors and rarely metastasis, it can be locally aggressive in nature [1] with a high destructive potential, affecting the surrounding structures including bone and vital organs (eyelids, earlobes, etc.).

Clinically, BCCs can have varied appearance based on their histopathological subtypes. Nodular BCCs (nBCC) are the most common subtypes accounting for 80% of the lesions [4]. They are primarily located on the face. Clinically, they present as shiny papules or nodules, which may have "rolled" borders and telangiectatic vessels. Superficial BCCs (sBCC) are mostly located on upper trunk and appears as slightly scaly plaques, pink to flesh-colored. Morpheaform or sclerosing BCCs are typically located in the mid-facial sites and appears as scar-like lesions with ill-distinct borders. Ulceration is a usual feature for all BCCs subtypes, and pigmentation can also be seen.

Dermoscopy is useful for the diagnosis of BCC. Several dermoscopic features of BCC have been described: large blue-grey ovoid nests, multiple blue-grey dots and globules, leaf-like areas, spoke wheel areas, concentric structures, arborizing vessels, short fine telangiectasias, shiny white and white-red structures, ulceration, multiple small erosions, and shiny white-red structureless areas [5].

On histopathology, there are various subtypes of BCCs. The most common subtypes including nBCC, sBCC, micronodular BCC, infiltrative BCC (iBCC), morpheaform or sclerosing BCCs, and infundibulocystic BCCs. nBCCs and sBCCs consist of varied sized nests of basaloid cells with peripheral palisading and clefting located in the dermis and attached to the basal layer of epidermis, respectively. Around the tumor nests, mucinous stroma can be seen. In iBCC, small irregular clusters of basaloid cells are seen in the dermis. Micronodular BCC is characterized by small

M. Sendín-Martín
Dermatology Department, Hospital Universitario Virgen del Rocío, Sevilla, Spain

U. Harris · M. Moronta · E. Lee · A. Rossi · C.-S.J. Chen · K. Nehal · M. Jain (✉)
Dermatology Service, Department of Medicine, Memorial Sloan Kettering Cancer Center (MSKCC), 530 E. 74th Street, New York, NY, USA
e-mail: jainm@mskcc.org

M. Pulitzer
Department of Pathology, Memorial Sloan Kettering Cancer Center (MSKCC), New York, NY, USA

M. Jain et al. (eds.), *Cutaneous Atlas of Ex Vivo Confocal Microscopy*,
https://doi.org/10.1007/978-3-030-89316-3_7

Table 7.1 Basics of basal cell carcinoma (BCC)

• **Epidemiology and patients demographics**: BCC is the most common skin cancer, with rising incidence [13]. Predominantly seen in older adults with fair skin phototype (I to III), characteristically in sun-exposed body sites.
• **Etiology**: UV exposure, childhood and adolescent sun exposure, radiation, genetics (PTCH, p53, BAX gene mutations).
• **Clinical Presentation**: Nodular BCCs are pink or flesh-colored papules with pearly quality, and often with telangiectatic vessel. Ulceration is frequent. Superficial BCCs typically present as slightly scaly plaques, light red to pink in color. Morpheaform or sclerosing BCCs usually present as atrophic plaques with ill-defined borders.
• **Dermatoscopy**: Large blue-grey ovoid nests, multiple blue-grey dots and globules, leaf-like areas, spoke wheel areas, concentric structures, arborizing vessels, short fine telangiectasias, shiny white and white-red structures, ulceration, multiple small erosions, shiny white-red structureless areas [5].
• **Histolopathology**: Several subtypes have been described. The most common subtypes are nodular (50–80%) and superficial (10–30%). Otherless common BCC subtypes (<10%) include infiltrative, morpheaform, infundibulocystic, fibroepithelial, or basosquamous patterns. Most of the BCCs exhibit more than one histopathologic pattern [3].

basaloid nests; while, sclerosing BCC have thin strands of basaloid cells embedded within a dense sclerotic stroma.

Mohs micrographic surgery (MMS) is a specialized surgical procedure designed to treat and achieve complete clearance of BCCs. MMS provides high cure rates [6] and allows surgeons to maximize tissue preservation while treating recurrent BCCs or BCCs located in the cosmetic sites, such as the face [7]. Frozen sections performed during MMS is a time consuming ($\sim$ 20 to 40 min /layer removal) and a labor intensive [8] process, which is currently a major limitation of this procedure.

Ex vivo confocal microscopy (EVCM) is an attractive alternative to frozen sectioning during Mohs surgery as it can rapidly image fresh (unprocessed and un-sectioned) tissue, enabling tumor margin assessment in real-time. EVCM has shown high sensitivity and specificity for detecting BCCs in fresh Mohs surgical excisions in several studies [9–12], paving the way to a future rapid bedside histopathologic guidance for the surgeons.

In this chapter, we have described the morphological features of common subtypes of BCC as visualized in various imaging modes on the EVCM device, including fluorescence confocal microscopy (FCM) mode and digital H&E (DHE) mode and compared them with their corresponding H&E-stained frozen sections (Table 7.2). For image acquisition, the latest generation of EVCM device (Vivascope 2500; Caliber ID, Rochester, NY, USA) was used to image fresh discarded BCC tissues from MMS (Figs. 7.1, 7.2, 7.3, 7.4, 7.5, 7.6, 7.7, 7.8, 7.9, 7.10, 7.11, 7.12, 7.13, 7.14 and 7.15).

Table 7.2 Morphological features of BCCs on FCM, and DHE modes and comparison with their corresponding histopathology

Fluorescence confocal microscopy (FCM) mode (grayscale image) [7, 11] (Figs. 7.1a, 7.2a, 7.3a, 7.4a, 7.5a, 7.6a, 7.7a, 7.8a, 7.9a, 7.10a, 7.11a, 7.12a, 7.13a, 7.14a and 7.15a)	Digital H&E (combined FCM and RCM modes) (Figs. 7.1b, 7.2b, 7.3b, 7.4b, 7.5b, 7.6b, 7.7b, 7.8b, 7.9b, 7.10b, 7.11b, 7.12b, 7.13b, 7.14b and 7.15b)	Conventional H&E-stained image (Figs. 7.1c, 7.2c, 7.3c, 7.4c, 7.5c, 7.6c, 7.7c, 7.8c, 7.9c, 7.10c, 7.11c, 7.12c, 7.13c, 7.14c and 7.15c)
Fluorescence: BCC nuclei visualized as bright white structures with 1000-fold enhanced contrast compared to the surrounding dermis	Fluorescent nuclear signal appears dark purple in DHE images	The bright signal on FCM and dark purple color on DHE corresponds to hematoxylin-stained hyperchromatic nuclei of BCC
Tumor demarcation: Tumor shape can be clearly drawn to separate bright cell nuclei in the tumor nodule from rest of the grayish dermis	**Tumor demarcation**: Dark purple tumor nodules appear well-demarcated in the background of pinkish collagen	**Tumor demarcation**: Tumor nodules of basaloid cells (bright on FCM; purple on DHE) can be readily identified in the dermis (grayish on FCM; pinkish on DHE)
Nuclear crowding: Higher nuclear density within the tumor nodule makes neoplastic islands appear bright	**Nuclear crowding**: Nuclear crowding appears as dark purple color nuclei within the BCC nodules	**Nuclear crowding**: Crowded nuclei of BCC nodules are hematoxylin-stained (bright on FCM; dark purple on DHE)
Peripheral palisading: Parallel arrangement of bright cells at the periphery of the tumor nodule	**Peripheral palisading**: Parallelly arranged dark purple nuclei at the periphery of the BCC nodules	**Peripheral palisading**: Hematoxylin-stained basaloid nuclei (bright on FCM; purple on DHE) at the periphery of BCC nodules
Clefting: Fluorescence-free (nonfluorescent) dark half-moon attached to the bright tumor mass	**Clefting**: Appears as white area adjacent to the dark purple BCC nodules	**Clefting**: Retraction space between tumor and the surrounding stroma created by washing off the mucin during tissue processing (dark on FCM; white on DHE)
Nuclear pleomorphism: Aberrant hyperfluorescent nuclei visualized as bright white structures	**Nuclear pleomorphism**: Varied size and shaped dark purple nuclei within the BCC nodules	**Nuclear pleomorphism**: Hematoxylin-stained tumor nuclei (bright on FCM dark purple on DHE) of varied in size and shape within the BCC nodules
Enlarged N/C ratio: BCC nests are visualized as enlarged bright (hyperfluorescent) masses with surrounding scant grayish (hypofluorescent) cytoplasm	**Enlarged N/C ratio**: Tumor cells have enlarged dark purple nuclei with scant pale pink cytoplasm	**Enlarged N/C ratio**: Higher nuclear/cytoplasmic ratio of BCC tumor cells (bright on FCM; dark purple on DHE) as compared to the normal keratinocytes
Tumoral Stroma: Within the tumor stroma inflammatory infiltrate may be visualized as bright (hyperfluorescent) dots in a dark (nonfluorescent/ hypofluorescent) background. This pattern is known as *"starry sky"* stroma	**Tumoral Stroma**: Inflammatory cells appear as purple small scattered or clustered dots within a pale pink collagen and can be easily distinguished from the dark purple and enlarged nuclei of BCC	**Tumoral Stroma**: Hematoxylin-stained lymphocytes (bright on FCM; purple on DHE) seen in the stroma surrounding the BCC nodules

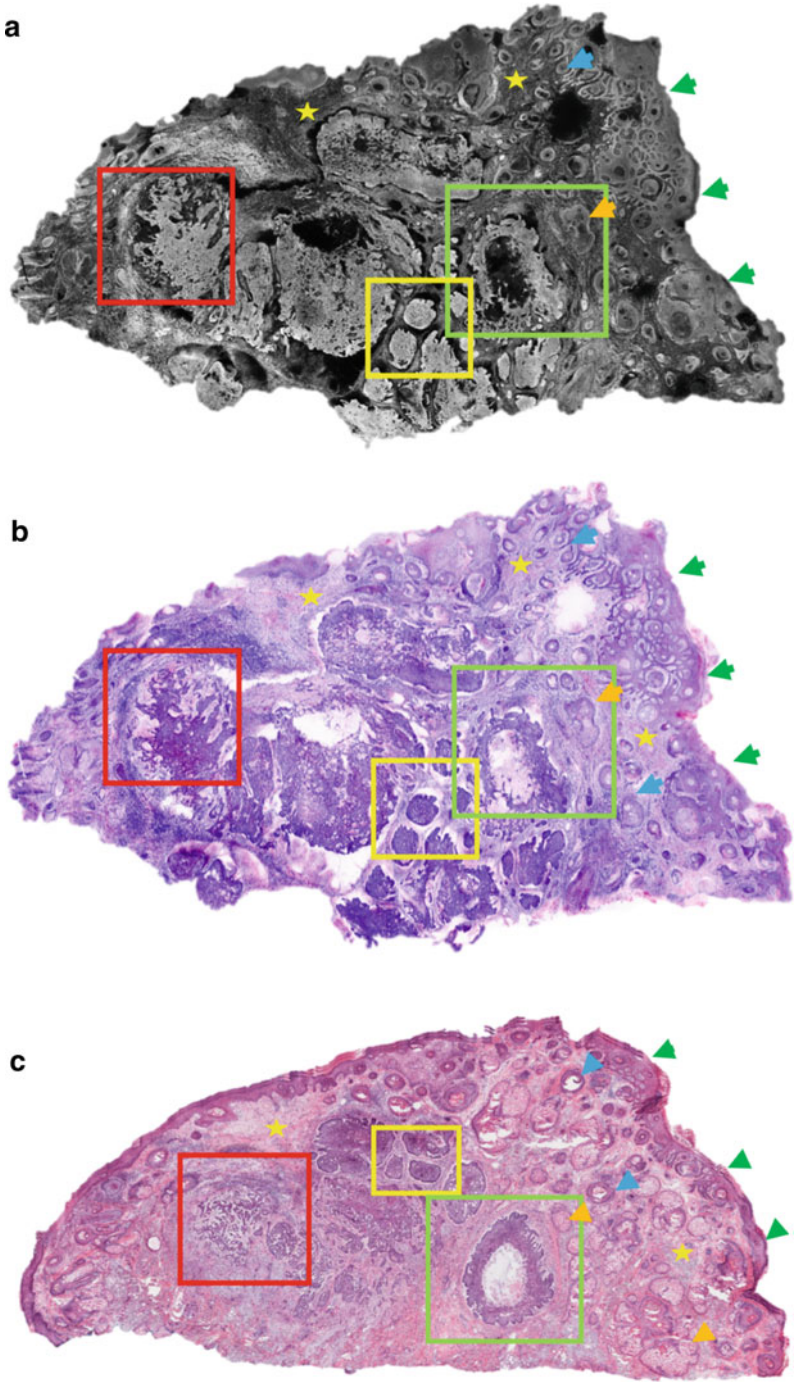

Fig. 7.1 Low magnification mosaic images of a nodular and infiltrative BCC from left nasal ala of an 84-year-old male. **a** FCM image shows well demarcated bright tumor nodules (boxed areas) within a grayish white dermis (yellow stars). These nodules can be clearly differentiated from the surrounding grayish white normal skin structures of hair follicles (blue arrows), sebaceous glands (orange arrow), and epidermis (green arrows). **b** On the corresponding digital H&E (DHE) image, BCC tumor nodules (boxed areas) appear as dark purple (bright on FCM) aggregates of varied sizes within a purplish pink (grayish white on FCM) dermis (yellow stars). These tumor nodules can be readily distinguished from the surrounding hair follicles (blue arrows), sebaceous glands (orange arrow), and epidermis (green arrows). **c** Corresponding conventional H&E stained image shows an excellent correlation with FCM (**a**) and DHE (**b**) images for the BCC tumor nodules (boxed areas), dermis (yellow stars), hair follicles (blue arrows), sebaceous glands (orange arrow), and epidermis (green arrows). H&E magnification = 2X

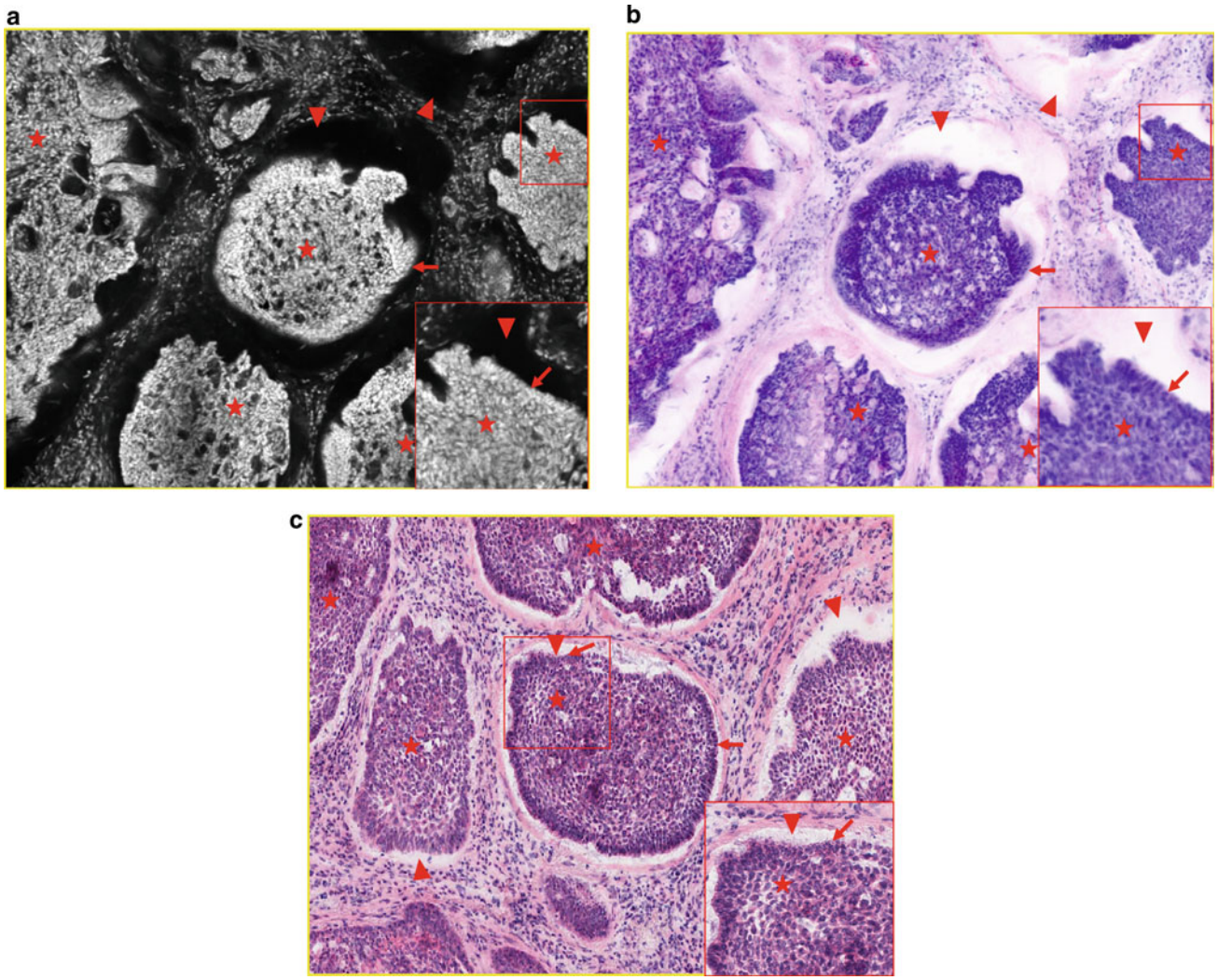

Fig. 7.2 Medium and high magnification submosaic images of nodular BCC showing cellular features obtained by digitally zooming in the yellow boxed area of mosaics in Fig. 7.1. **a** FCM image shows bright (hyperfluorescent) tumor nodules of BCC (red stars) composed of crowded nuclei with increased N:C ratio (inset). These bright nuclei form peripheral palisading (red arrow and inset) at the tumor periphery. Around each tumor nodule, clefting (red arrowheads and inset) appears as a dark space. **b** Corresponding digital H&E image shows these tumor islands (red stars) as dark purple (bright on FCM) well-defined aggregates. Tumor cells (inset) have nuclear pleomorphism and a high N:C ratio forming peripheral palisading (red arrow, red box). Clefting (red arrowheads) appears as a white space (dark on FCM) around individual tumor nodule. **c** Corresponding conventional H&E-stained image shows a good correlation with the FCM (**a**) and DHE (**b**) images for cellular features of the nodular BCC (red stars and inset) including palisading (red arrow and inset), and surrounding clefting (red arrowheads and inset). H&E magnifications = 10X, 20X (inset)

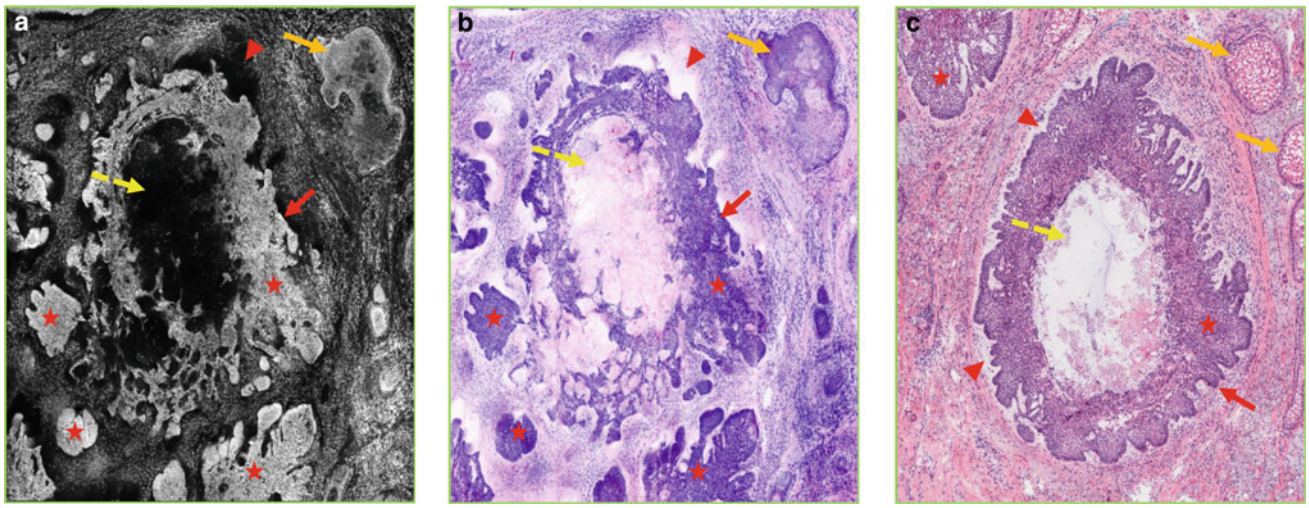

Fig. 7.3 Medium magnification submosaic images of a nodular BCC showing cystic degeneration obtained by digitally zooming in green boxed area of mosaics in Fig. 7.1. **a** FCM image shows bright well-demarcated tumor aggregates of nodular BCCs (red stars) with peripheral palisading (red arrow) and dark surrounding clefting (red arrowhead). The tumor nodule shows central dark area of cystic degeneration (yellow dashed arrow). These BCC tumor nodules appear distinct from the surrounding sebaceous gland (orange arrow) which appears less bright and lacks cellular features of BCC (enlarged N/C ratio, nuclear crowding, and palisading) and clefting. **b** On the corresponding digital H&E (DHE) image, BCC tumor nodules (red stars) appear as dark purple (bright on FCM) aggregates with palisading (red arrow) and the clefting (red arrowheads) appears as white space (dark on FCM). The cystic degeneration tumor necrosis (yellow dashed arrow) appears as pale pink (dark on FCM) acellular area. Sebaceous gland (orange arrow) appears pale purple in color (less bright on FCM). **c** Corresponding conventional H&E stained image shows an excellent correlation with FCM (**a**) and DHE (**b**) images for the BCC tumor nodules (red stars) with palisading (red arrow), clefting (red stars), and central necrosis (yellow dashed arrow), and for the sebaceous glands (orange arrows). H&E magnifications = 10X

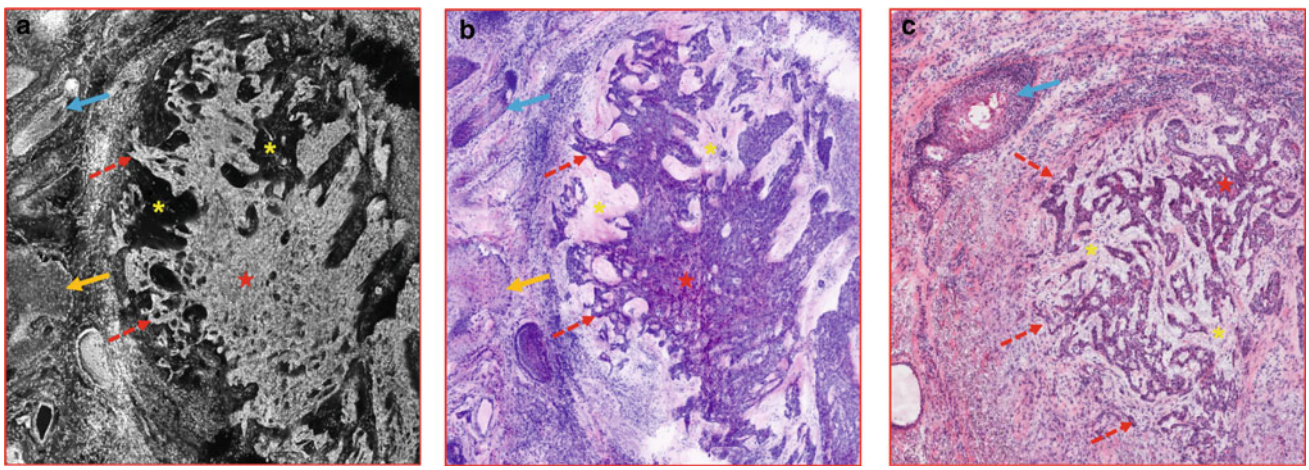

Fig. 7.4 Medium magnification submosaic images of a nodular infiltrative BCC with surrounding mucin obtained by digitally zooming in red boxed area of mosaics in Fig. 7.1. **a** FCM image shows a bright BCC tumor nodule (red star) with irregular cords at the periphery (red dashed arrows), which is surrounded by a dark area of mucin (yellow asterisks). The sebaceous gland (orange arrow) and hair follicle (blue arrow) have a sparse less bright smaller nuclei as compared to the nuclei of BCC. **b** On the corresponding digital HE (DHE) image, BCC nodule (red star) and cords (red dashed arrows) appears dark purple (bright on FCM). The surrounding mucin (yellow asterisks) is visualized as pale pink (dark on FCM) homogenous area (red asterisks). Sebaceous gland (orange arrow) and hair follicle (blue arrow) can be clearly visualized. **c** Corresponding conventional H&E stained image shows an excellent correlation with the FCM (**a**) and DHE (**b**) images for the features of BCC (red star) with mostly infiltrative cords (red dashed arrows), surrounding mucin (yellow asterisks) and a pilosebaceous unit (blue arrow). Note, nodular pattern of BCC is not evident on H&E due to a relatively deeper section. H&E magnification = 10X

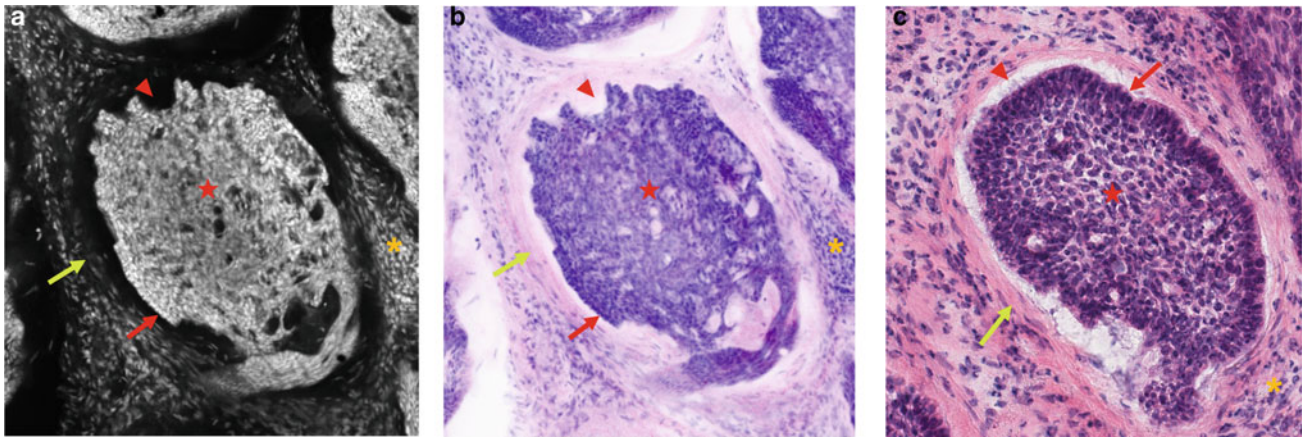

Fig. 7.5 High magnification submosaic images of another nodular BCC showing surrounding collagenous stroma. **a** FCM image shows a bright well-demarcated BCC tumor nodule (red star) with cellular features of BCC, including peripheral palisading (red arrow). Around the nodule, one can appreciate organized bundles of grayish collagen fibers (fluorescent green arrow) and a foci of inflammatory cells (orange asterisk). **b** On the corresponding digital H&E (DHE) image, the nodule (red star) appears well-demarcated and dark purple (bright on FCM) in color with cellular features of BCC and palisading. The organized collagen fibers (fluorescent green arrow) appears pink (grayish on FCM) and inflammatory foci (orange asterisk) appears purple in color (bright on FCM). **c** Corresponding conventional H&E-stained image shows an excellent correlation with the FCM (**a**) and DHE (**b**) images for the BCC tumor nodule (red star) with palisading (red arrow), and surrounding collagen bundles (fluorescent green arrow) and inflammation (orange asterisk). H&E magnification = 40X

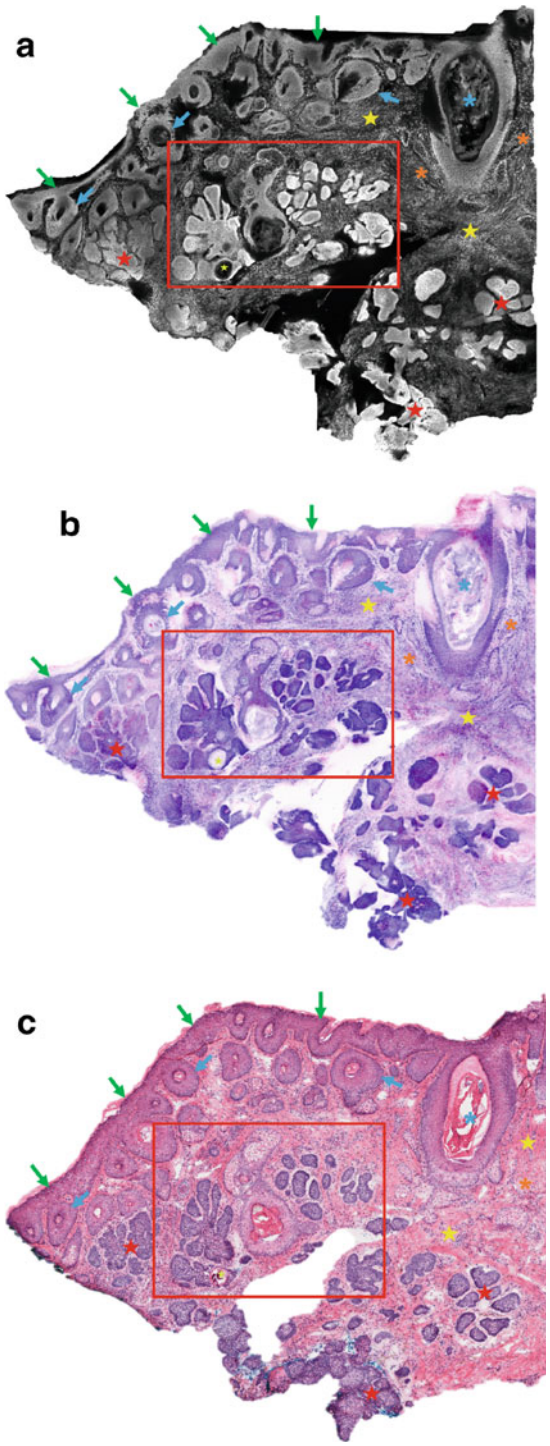

Fig. 7.6 Low magnification submosaic images of a nodular BCC showing focal keratinization obtained from left nasal ala of a 34-year-old male. **a** FCM image shows well-demarcated bright and crowded aggregates of BCC tumor nodules (red stars and red boxed area) that can be readily distinguished from the less bright surrounding hair follicles (blue arrows), and epidermis (green arrows). Within one of the tumor nodule, a grayish dark cyst-like space (fluorescent green star) can be seen. One of the hair follicle infundibulum is dilated and is filled with grayish material (blue asterisk). The surrounding grayish dermis (yellow stars) has extensive inflammatory infiltrate of small bright cells (orange asterisks). **b** On the corresponding DHE image, aggregates of nodular BCC (nBCC; red boxed area and red stars) appears dark purple in color (bright on FCM) BCC, while the hair follicles (blue arrows) and epidermis (green arrows) appears paler purple (less bright on FCM). The dark cyst-like space (fluorescent green star) within the tumor nodule appears as lamellated pale purple keratin (grayish dark on FCM). The keratin within the dilated hair infundibulum (blue asterisk) also appears purplish in color (blue asterisk). Inflammatory infiltrate (orange asterisks) appears as small purple (bright on FCM) dots in a pinkish (grayish on FCM) dermis (yellow stars). **c** Corresponding conventional H&E stained image shows correlative features with the FCM (**a**) and DHE (**b**) images for the BCC tumor nodules (red stars and boxed area) with focal keratinization (fluorescent green star), hair follicles (blue asterisk), dilated hair follicle infundibulum (blue star), epidermis (green arrows), and Inflammatory infiltrate (orange asterisk) in the dermis (yellow stars). H&E magnifications = 4X

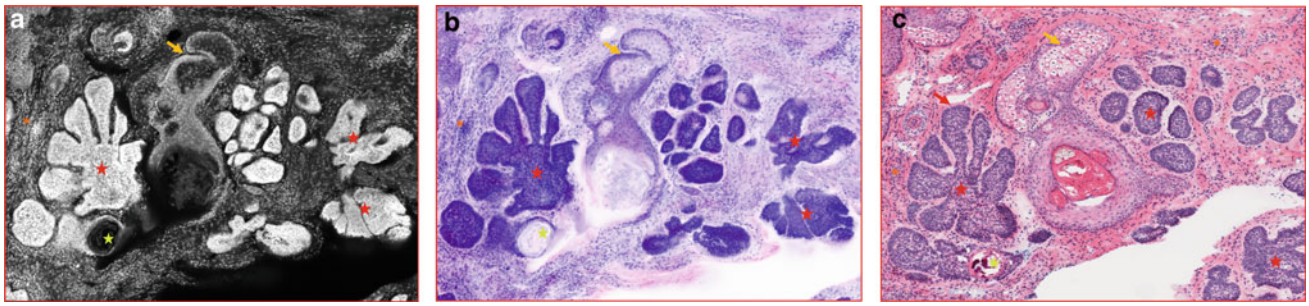

Fig. 7.7 High magnification submosaic images of the nodular BCC with focal keratinization obtained by digitally zooming in the red boxed area of mosaics in Fig. 7.6. **a** FCM image shows well-demarcated bright and crowded aggregates of BCC tumor nodules (red stars) with grayish dark cyst-like space (fluorescent green star) in the center of one of the nodules. Small bright inflammatory cells (orange asterisk) are seen surrounding the tumor nodules. A pilosebaceous gland (orange arrow) can be easily distinguished from the adjacent BCC tumor nodules. **b** On the corresponding digital H&E (DHE) image, the tumor aggregates of BCC (red stars) appears dark purple (bright on FCM) and the central keratinization (fluorescent green star) appears as lamellated pale purple (grayish dark on FCM) material. The inflammatory cells clusters (orange asterisk) appears purple in color (bright on FCM) and the pilosebaceous gland (orange arrow) as pale purple. **c** Corresponding conventional H&E-stained image, correlates well with the FCM (**a**) and DHE (**b**) images for BCC tumor nodules (red stars) with keratinization (fluorescent green star), inflammatory cells (orange asterisk), and pilosebaceous gland (orange arrow). H&E magnifications = 10X

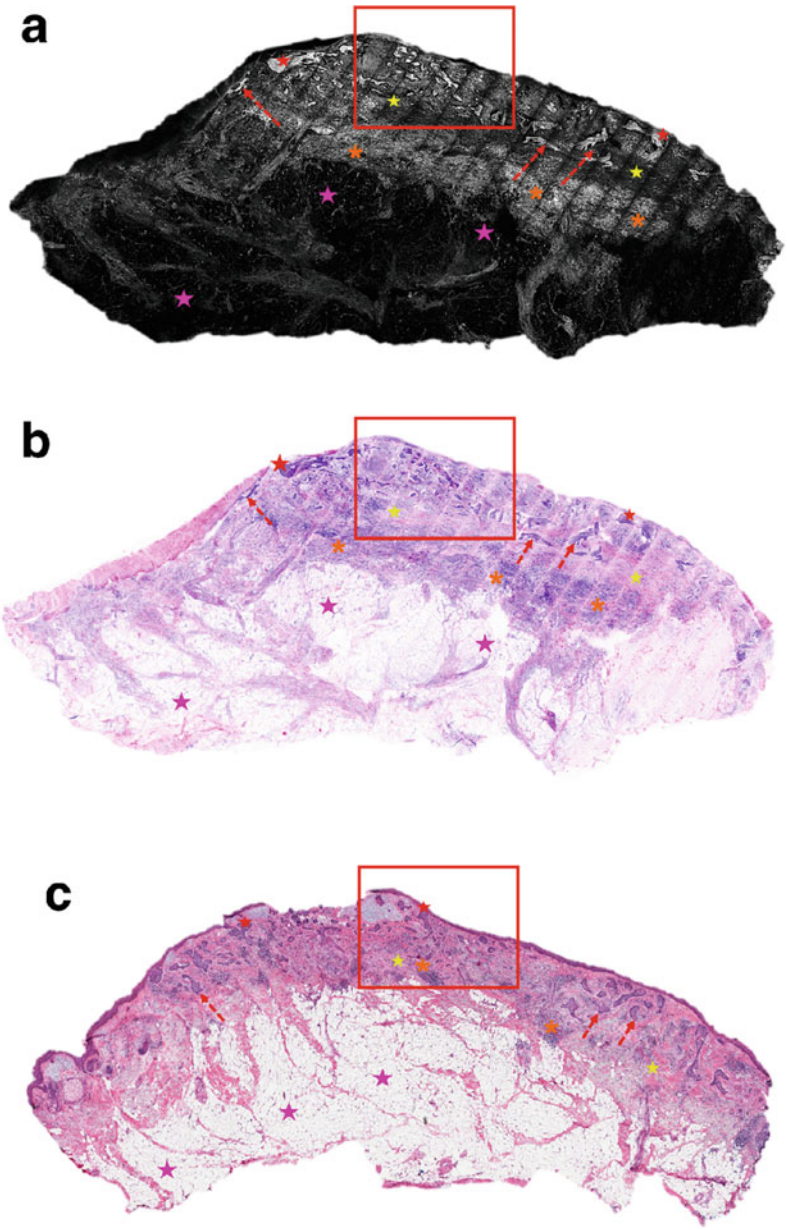

Fig. 7.8 Low magnification mosaic images of a nodular and infiltrative BCC (nBCC and iBCC) obtained from right cheek of a 95-year-old male. **a** FCM image shows larger bright tumor aggregates (red boxed area, and red stars) of nBCC and bright thin irregular strands (red dashed arrows) of iBCC in the grayish dermis (yellow stars). Even at this low magnification, the thin bright strands of iBCC can be readily identified within the "starry sky" appearance of inflammatory cells (orange asterisks). Subcutis appears as dark lobules (pink stars) and is free from BCC infiltration. **b** On the corresponding DHE image, both the large aggregates (red stars) of nBCC and thin strands of iBCC (red dashed arrows) appears as dark purple in color (bright on FCM) within a purplish pink (grayish on FCM) dermis (yellow stars). The inflammatory cells (orange asterisks) appears as clusters of small purple color (bright on FCM) dots, which can be readily distinguished from the thin iBCC strands (red dashed arrows). Subcutis (pink stars) appears as white lobulated (dark on FCM) structures of adipocytes. **c** Corresponding conventional H&E-stained image demonstrates an excellent correspondence with the FCM (**a**) and DHE (**b**) images for the nodular (red star) and infiltrative components of BCC (red boxed area and red dashed arrows), and for the surrounding dermis (yellow stars) with inflammation (orange stars), and the subcutis (pink stars). H&E magnifications = 2X

Fig. 7.9 Medium magnification submosaic images of the nodular and infiltrative BCC showing cellular features obtained by digitally zooming in the red boxed area from the mosaics in Fig. 7.8. **a** FCM image shows both the nodular (red stars) and infiltrate BCC (red dashed arrows) as bright tumor aggregates within a relatively dark grayish dermis (yellow star). Nodular BCC (red stars) is surrounded by dark areas of clefting (red arrowheads). Within the tumor aggregates, crowded and bright nuclei forms peripheral palisading (red arrows). Palisading and clefting are less distinct around the thin strands of iBCCs; however, these tumor strands can be readily distinguished from surrounding small bright inflammatory cell aggregates (orange asterisks) due to their angulated and irregular shape. In the superficial dermis, a grayish crumpled area of solar elastosis (purple asterisk) can be seen. Epidermal nuclei (green arrows) appear less bright and less crowded compared to the BCCs. **b** On the corresponding DHE image, nBCC (red stars) and iBCC (red dashed arrows) appears as dark purple (bright on FCM) large aggregates (red stars) and thin irregular strands (red dashed arrows), respectively. Solar elastosis (purple asterisk) appear as crumpled pale purple (grayish on FCM) material in the dermis (yellow star). Inflammatory cells (orange asterisks) appears purple (bright on FCM). **c** Corresponding conventional H&E-stained image shows an excellent correlation with FCM (**a**) and DHE (**b**) images for the morphological features of nBCC (red stars) and iBCC (red dashed arrows), clefting (red arrowheads), palisading (red arrow), epidermis (green arrows), inflammatory cells (orange asterisks), and solar elastosis (purple asterisk). H&E magnifications = 10X

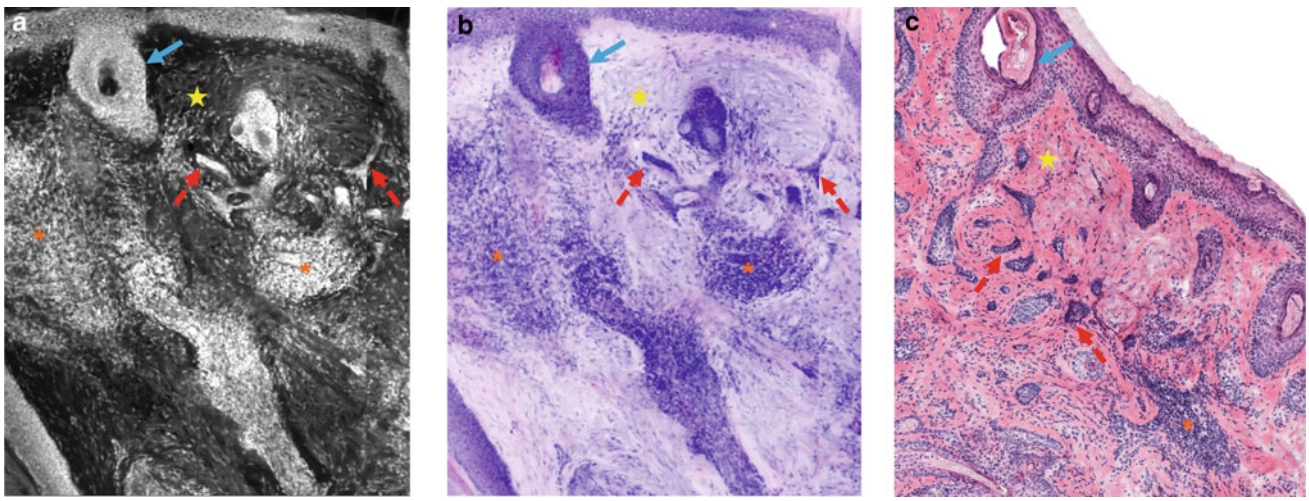

Fig. 7.10 Medium magnification submosaic images of another infiltrative BCC (iBCC) showing subtle thin tumor strands obtained from left supra nasal tip of a 74-year-old female. **a** FCM image shows thin bright strands of iBCC (red dashed arrows), which can be readily discerned in extensive bright inflammatory cell clusters (orange asterisks) within a grayish dark dermis (yellow star). A hair follicle (blue arrow) can also be identified. **b** Digital HE image shows these thin strands (red dashed arrows) as dark purple in color (bright on FCM) in the surrounding pinkish purple (grayish on FCM) dermis (yellow star). These cohesive thin strands of iBCC can be readily contrasted from the surrounding dense purple color (bright on FCM) inflammatory infiltrate (orange asterisks). The hair follicle (blue arrow) appears pale purple in color. **c** Corresponding conventional H&E-stained image shows a close correspondence with the FCM (**a**) and DHE (**b**) images for iBCC strands (red dashed arrows), inflammatory cells (orange asterisk) in dermis (yellow star), and a hair follicle (blue arrow). H&E magnifications = 10X

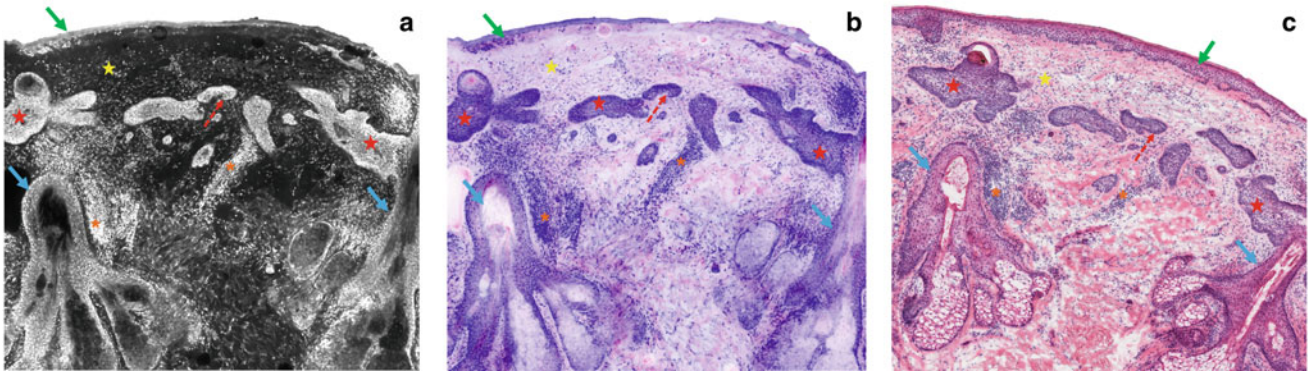

Fig. 7.11 Medium magnification mosaic images of another nodular and infiltrative BCC (nBCC and iBCC) showing perifollicular origin obtained from left scalp of a 69-year-old male. **a** FCM image shows bright tumor aggregates of nBCC (red stars) and infiltrative BCCs (red dashed arrow). One of the nodules, on the right side of the image, is seen originating from the lining of a pilosebaceous gland (blue arrow). Overlying epidermis (green arrow) is bright with sparse nuclei in comparison to the crowded nuclei of BCC aggregates (red stars and red dashed arrow). In the grayish dark dermis (yellow star), bright clusters of inflammatory cells (orange asterisks) are identified. **b** On the corresponding digital (H&E) image, the tumor nodules (red stars) and infiltrative BCCs strands (red dashed arrow) appears dark purple in color (bright on FCM). Perifollicular (blue arrows) involvement by one of the larger dark purple nodule (red star) is evident. Epidermis (green arrow) has small purple sparse nuclei, while clusters of small purple (bright on FCM) inflammatory cells (orange asterisks) stands out in purplish pink (yellow star). **c** Corresponding conventional H&E stained tissue section shows close resemblance to the DHE (**a**) image for superficial and infiltrative BCC components (red stars) within the dermis (yellow asterisk), inflammatory cells (orange asterisks), pilosebaceous glands (orange arrows) and hair follicles (blue arrows) and overlying epidermis (green arrow). H&E magnifications = 10X

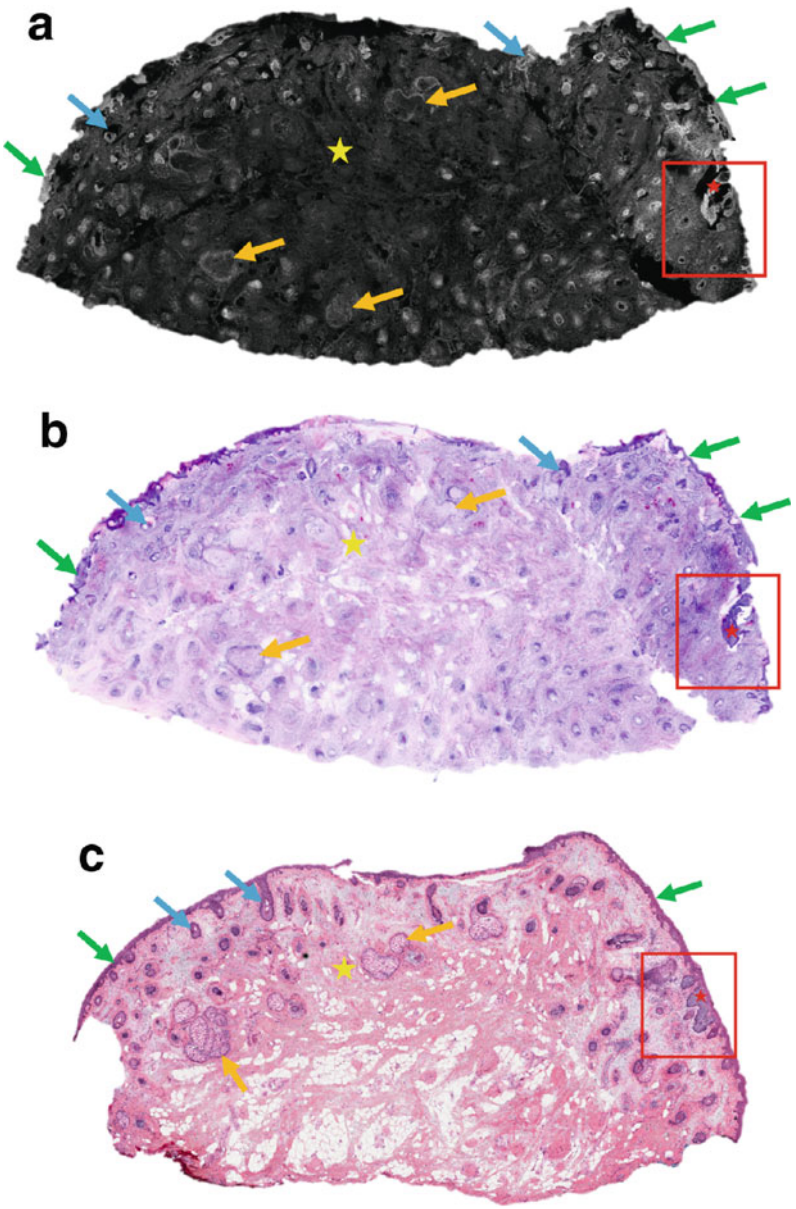

Fig. 7.12 Low magnification mosaic images of a superficial BCC obtained from right cheek of a 60-year-old male. **a** FCM image shows a bright well-demarcated sBCC tumor aggregate (red star and red boxed area) originating from the overlying normal epidermis (green arrows). Even at this scanning magnification tumor aggregate appears distinct from the relatively less bright epidermis and other normal structures such as sebaceous glands (orange arrows) and hair follicles (blue arrows). Dermis appears grayish dark (yellow star). **b** On the corresponding DHE, sBCC tumor nodule (red star, red boxed area) appears dark purple in color (bright on FCM). Sebaceous glands (orange arrows), hair follicles (blue arrows), and epidermal nuclei (green arrows) appear less intense purple in color (less bright on FCM) and can be readily distinguished from the dark purple aggregate of sBCC. Dermis appears pinkish purple (grayish dark on FCM). **c** Corresponding conventional H&E stained image shows an excellent correspondence to the sBCC tumor foci (red star and red boxed area), sebaceous gland (orange arrows), hair follicles (blue arrows), dermis (yellow star), and overlying epidermis (green arrows). H&E magnifications = 4X

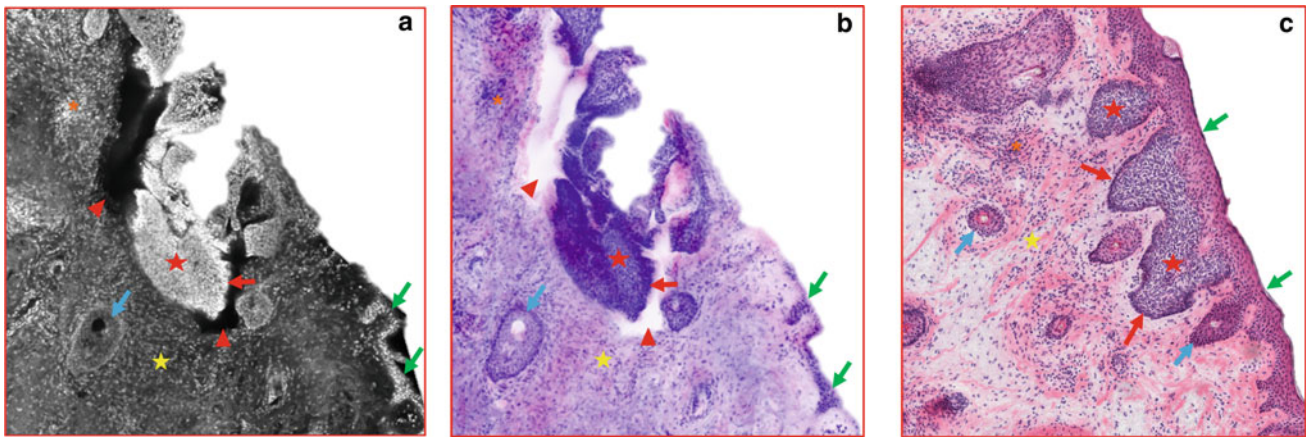

Fig. 7.13 High magnification submosaic images of the superficial BCC showing cellular features obtained by digitally zooming in the red boxed area from the mosaics in Fig. 7.12. **a** FCM image shows a bright tumor aggregate of superficial BCC (sBCC) (red star) with high N:C ratio, nuclear crowding, and peripheral palisading (red arrow). Surrounding this bright tumor aggregate is a dark area of clefting (red arrowheads). This bright tumor aggregate can be readily distinguished from the sparsely nucleated and less bright epidermis (green arrows), and hair follicles (blue arrow). There is a sprinkle of bright small cells inflammatory cells (orange asterisk) throughout the grayish dermis (yellow stars). **b** On the corresponding DHE image, aggregate of sBCC (red star) appears dark purple (bright on FCM) and well-defined. The cellular features of increased N:C ratio, overcrowded nuclei, and peripheral palisading (blue arrow) are distinct. This tumor aggregate appears distinct from the normal epidermis (green arrows) and hair follicle (blue arrow) which have sparse and lighter purple (less bright on FCM) nuclei. Hugging the lower edge of this tumor nodule is a whitish space (dark on FCM) that corresponds to clefting (red arrowheads). Inflammatory cells (orange asterisk) appears as small purple color (bright on FCM) dots in the dermis (yellow star). **c** Corresponding conventional H&E stained image shows correlative cellular features of sBCC (red stars) including peripheral palisading (red arrow), normal epidermis (green arrows), hair follicles (blue arrow), and dermal (yellow star) inflammatory cells (orange asterisk). H&E magnifications = 20X

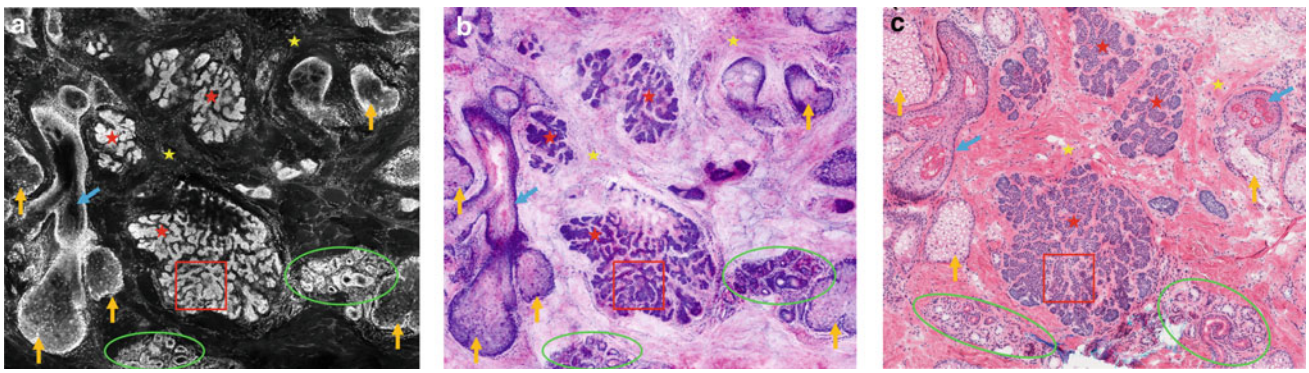

Fig. 7.14 Medium magnification submosaic images of an infundibulocystic BCC obtained from right lower canthus of a 59-year-old male. **a** FCM image shows a multiple tumor foci with anastomosing cords and strands (red stars) within a grayish dark dermis (yellow stars). These tumor cords and strands can be clearly distinguished from the surrounding hair follicles (blue arrow), sebaceous glands (orange arrows), and eccrine ducts (fluorescent green circles). **b** On the corresponding DHE image, clusters of tumor cords and strands (red stars) appears dark purples (bright on FCM) within a pinkish (grayish on FCM) dermis (yellow stars). The hair follicle (blue arrow), and sebaceous glands (orange arrows) appears paler purple with sparse nuclei, while the eccrine ducts (fluorescent green circles) appears dark purple but with less nuclear crowding than BCC. **c** Corresponding conventional H&E-stained image shows an excellent correlation with the FCM (**a**) and DHE (**b**) images for the tumor (red stars), hair follicle (blue arrow), sebaceous glands (orange arrows), eccrine ducts (fluorescent green circles) and dermis (yellow stars). H&E magnifications = 10X

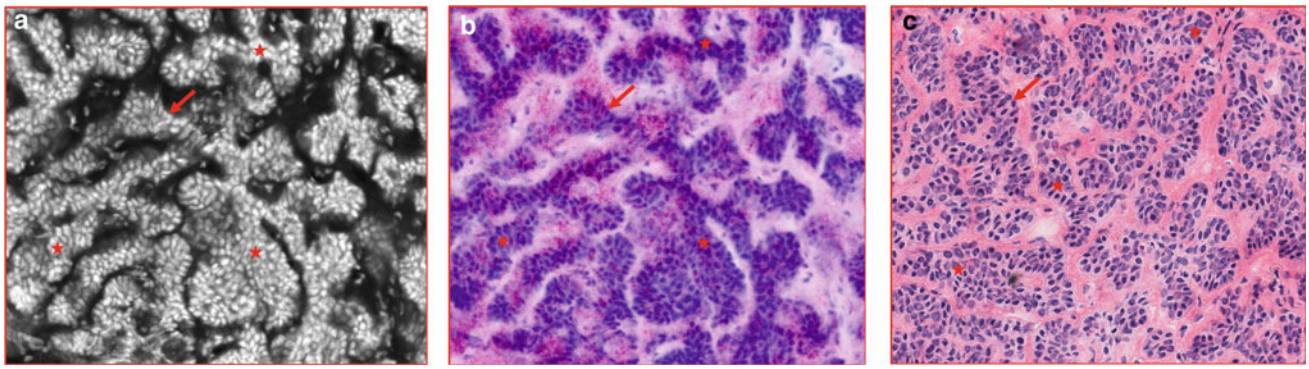

Fig. 7.15 High magnification submosaic images of the infundibulocystic BCC showing cellular features obtained by digitally zooming in the red boxed area in Fig. 7.14. **a** FCM image shows bright anastomosing cords and strands of BCC (red stars) composed of nuclei with increased N:C ratio and peripheral palisading (red arrows). **b** On the corresponding digital HE (DHE) image, these cords and strands of BCC (red stars) appears dark purple composed of nuclei with increased N:C ratio and peripheral palisading (red arrows). **c** Corresponding conventional H&E-stained image shows an excellent correlation with the FCM (**a**) and DHE (**b**) images for the cellular details of BCC (red arrowheads). H&E magnifications = 40X

References

1. Nehal KS, Bichakjian CK. Update on keratinocyte carcinomas. N Engl J Med. 2018;379:363–74. https://doi.org/10.1056/NEJMra1708701.
2. Asgari MM, Moffet HH, Ray GT, Quesenberry CP. Trends in basal cell carcinoma incidence and identification of high-risk subgroups, 1998–2012. JAMA Dermatol. 2015;151:976–81. https://doi.org/10.1001/jamadermatol.2015.1188.
3. Cameron MC, Lee E, Hibler BP, Barker CA, Mori S, Cordova M, et al. Basal cell carcinoma: epidemiology; pathophysiology; clinical and histological subtypes; and disease associations. J Am Acad Dermatol. 2019;80:303–17. https://doi.org/10.1016/j.jaad.2018.03.060.
4. Scrivener Y, Grosshans E, Cribier B. Variations of basal cell carcinomas according to gender, age, location and histopathological subtype. Br J Dermatol. 2002;147:41–7. https://doi.org/10.1046/j.1365-2133.2002.04804.x.
5. Reiter O, Mimouni I, Dusza S, Halpern AC, Leshem YA, Marghoob AA. Dermoscopic features of basal cell carcinoma and its subtypes: a systematic review. J Am Acad Dermatol. 2020. https://doi.org/10.1016/j.jaad.2019.11.008.
6. Van Loo E, Mosterd K, Krekels GAM, Roozeboom MH, Ostertag JU, Dirksen CD, et al. Surgical excision versus Mohs' micrographic surgery for basal cell carcinoma of the face: a randomised clinical trial with 10 year follow-up. Eur J Cancer. 2014;50:3011–20. https://doi.org/10.1016/j.ejca.2014.08.018.
7. Jain M, Rajadhyaksha M, Nehal K. Implementation of fluorescence confocal mosaicking microscopy by "early adopter" Mohs surgeons and dermatologists: recent progress. J Biomed Opt. 2017;22:24002. https://doi.org/10.1117/1.JBO.22.2.024002.
8. Rajadhyaksha M, Menaker G, Flotte T, Dwyer PJ, Âlez SG. Confocal examination of nonmelanoma cancers in thick skin excisions to potentially guide Mohs micrographic surgery without frozen histopathology. J Invest Dermatol. 2001;117:1137–43. https://doi.org/10.1046/j.0022-202x.2001.01524.x.
9. Karen JK, Gareau DS, Dusza SW, Tudisco M, Rajadhyaksha M, Nehal KS. Detection of basal cell carcinomas in Mohs excisions with fluorescence confocal mosaicing microscopy. Br J Dermatol. 2009;160:1242–50. https://doi.org/10.1111/j.1365-2133.2009.09141.x.
10. Gareau DS. Feasibility of digitally stained multimodal confocal mosaics to simulate histopathology. J Biomed Opt. 2009;14:034050. https://doi.org/10.1117/1.3149853.
11. Bennàssar A, Carrera C, Puig S, Vilalta A, Malvehy J. Fast evaluation of 69 basal cell carcinomas with ex vivo fluorescence confocal microscopy. JAMA Dermatol. 2013;149:839. https://doi.org/10.1001/jamadermatol.2013.459.
12. Mu EW, Lewin JM, Stevenson ML, Meehan SA, Carucci JA, Gareau DS. Use of digitally stained multimodal confocal mosaic images to screen for nonmelanoma skin cancer. JAMA Dermatol. 2016;152:1335–41. https://doi.org/10.1001/jamadermatol.2016.2997.
13. Rubin AI, Chen EH, Ratner D. Basal-cell carcinoma. N Engl J Med. 2005;353:2262–9. https://doi.org/10.1056/NEJMra044151.